Dissipation-Driven Behavior of Nonpropagating Hydrodynamic Solitons Under Confinement

Leonardo Gordillo*
Departamento de Física, Facultad de Ciencias Físicas y Matemáticas, Universidad de Chile, Casilla 487-3, Santiago, Chile

Mónica A. García-Ñustes†
Instituto de Física, Pontificia Universidad Católica de Valparaíso, Avenida Brasil, Valparaíso, Casilla 2950, Chile
(Received 12 August 2013; published 25 April 2014)

We have identified a physical mechanism that rules the confinement of nonpropagating hydrodynamic solitons. We show that thin boundary layers arising on walls are responsible for a jump in the local damping. The outcome is a weak dissipation-driven repulsion that determines decisively the solitons' long-time behavior. Numerical simulations of our model are consistent with experiments. Our results uncover how confinement can generate a localized distribution of dissipation in out-of-equilibrium systems. Moreover, they show the preponderance of such a subtle effect in the behavior of localized structures. The reported results should explain the dynamic behavior of other confined dissipative systems.

DOI: 10.1103/PhysRevLett.112.164101 PACS numbers: 05.45.Yv, 47.35.Fg, 47.54.-r

Many dissipative systems can display localized structures after compensating energy losses with external forcing. These structures, known as dissipative solitons, can emerge under either steady or parametric forcing. The steady family, which comprehends classical convectons [1], has been widely analyzed (cf. Ref. [2]). The parametric family includes solitons in coupled-pendula chains [3], magnetic wires [4], optical fibers [5], Kerr-type oscillators [6], granular layers [7], and non-Newtonian fluids [8]. Fluid dynamics provides a fruitful field for systems supporting parametric localized structures. Hydrodynamic oscillons [9,10] and Hele-Shaw solitons [11] are illustrative examples. Nonetheless, the most representative parametric dissipative structure is the nonpropagating hydrodynamic soliton: a localized Faraday wave that emerges in large-aspect-ratio free surfaces [12].

The prototype amplitude equation for these systems in one dimension is the parametric and dissipative nonlinear Schrödinger (pd-NLS) equation [13]

$$i(\partial_t\psi + \mu\psi) = \nu\psi + 2|\psi|^2\psi + \partial_{xx}\psi + \gamma\psi^*. \quad (1)$$

The equation has been deduced from fundamental equations in several parametric dissipative systems including nonpropagating hydrodynamic solitons [14]. Here, $\psi(x,t)$ is a complex field that depends slowly on space and time while ψ^* denotes its complex conjugate. The parameters μ, ν, and γ account, respectively, for linear damping, detuning, and parametric forcing. All the functions and variables are dimensionless. If $\gamma > \mu$ and $\nu < 0$, the pd-NLS equation supports stable steady localized solutions,

$$\psi_\pm(x,t) = \pm i\delta \mathrm{sech}[\delta(x - x_0)]e^{(i/2)\sin^{-1}(\mu/\gamma)}, \quad (2)$$

provided that $\gamma^2 < \nu^2 + \mu^2$ [4]. The constant δ represents the soliton amplitude and is given by $\delta^2 = -\nu + (\gamma^2 - \mu^2)^{1/2}$ [4].

Solitons can be very stable even in the presence of other nearby solitons [12]. Experiments and numerical simulations of the pd-NLS equation have shown a rich complexity of the behavior of interacting pairs, e.g., attraction, repulsion, and bound steady and oscillating states [15–18]. The dynamics depend on the parameter region as well as on the signs of the pair's constituents [notice $\pm$ in Eq. (2)]. Similar features hold for states involving several solitons where spontaneous organization [19], multisoliton complexes [20], and coalescence [21,22] have been reported. Other authors have studied the interaction with other *objects*, such as depth gradients [23,24], impurities [25,26], and boundaries [16,27]. In this Letter, we report a type of interaction between solitons and walls that leads to a better characterization of nonpropagating hydrodynamic solitons under confinement. We show from fluid dynamics equations that a dissipative process taking place in lateral-wall boundary layers is crucial. Numerical simulations show that this process generates dramatic changes in the solitons' behavior at long time scales. Our model is widely consistent with previous and current experiments as it is able to capture the slow drift of nonpropagating solitons in finite containers from Ref. [24].

Consider a fluid layer filling a trough of length l and breadth $b \ll l$ up to a depth d. At rest, the free surface lies on the plane $z = 0$. Its position at time t in terms of the horizontal coordinates $\mathbf{r} = (x, y)$ is denoted as $\eta(\mathbf{r}, t)$ [see Fig. 1(a)]. A straightforward result of the inviscid linear theory of gravity waves is that the free surface supports normal modes of the form $\eta_{p,q}(\mathbf{r}, t) \sim \mathrm{Re}[\exp(i\omega_{p,q}t + i\mathbf{k}\cdot\mathbf{r})]$. The frequencies ω are given by the dispersion

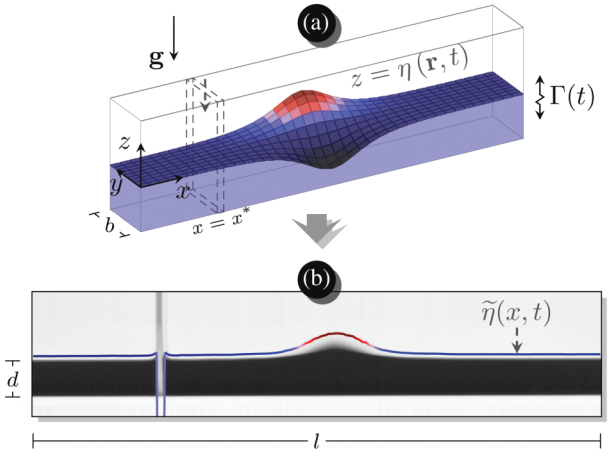

FIG. 1 (color online). (a) Scheme of a nonpropagating hydrodynamic soliton. The basin is shaken vertically at $\omega \lessapprox 2\omega_{0,1}$ while the soliton sloshes on the y axis at $\omega/2$. (b) Setup front view displaying a typical profile (see $\tilde{\eta}$ curve) extracted by image analysis. Slabs were used for analyzing soliton-wall interactions.

relation, $\omega_{p,q} = \sqrt{gk \tanh kd}$, where g is the gravity acceleration. The horizontal wave number $\mathbf{k}(k \equiv |\mathbf{k}|)$ should satisfy $\mathbf{k} = (\pi p/l, \pi q/b)$ with $(p, q) \in \mathbb{Z}^2$ to fulfill lateral boundary conditions [28]. In real experiments, normal modes decay due to dissipation. Notwithstanding this, they can be stabilized by applying vertical vibrations [29] at driving frequencies $\omega \approx 2\omega_{p,q}$ above a certain amplitude threshold [29]. This is true for all the modes except for $\eta_{0,1}$. Instead, and only after perturbing the surface, a sloshing waveform emerges [see Fig. 1(a)]. Its motion recalls the $\eta_{0,1}$ mode, but rather than involving the whole free-surface sloshing the wave localizes strongly in the longitudinal direction [12].

In the case of a nonpropagating hydrodynamic soliton, Eq. (1) stands for the longitudinal envelope of the first transverse mode $\tilde{\eta}(x, t)$, i.e., $\eta(\mathbf{r}, t) = \tilde{\eta}(x, t)\eta_{0,1}(y, t)$. The relations between the physical parameters and the detuning and parametric-forcing coefficients in Eq. (1) are given by $\nu = (\omega^2/\omega_{0,1}^2 - 1)/2$ and $\gamma = a_0/(4g)$, where a_0 is the acceleration forcing amplitude [14]. Expressions for the damping μ coefficient are displayed further below.

In finite domains, the pd-NLS equation requires the boundary conditions $\partial_x \psi|_{x=\{0,l\}} = 0$ to guarantee impermeability at lateral walls. In terms of interaction laws, this condition is analogous to considering a virtual-image soliton of the same sign at the other side of the boundary. This means that any soliton-wall interaction has a soliton-pair reciprocal interaction [27]. At least four types of same-sign soliton-pair interactions have been reported as forcing is increased: (a) the solitons merge into a single one, (b) the solitons merge and split periodically, (c) the solitons oscillate periodically (or quasiperiodically) without merging, and (d) the solitons form a steady state at a fixed distance [16,20,30]. Experimental evidence of reciprocal soliton-wall interactions is also available [27]. However, recent experiments have reported a puzzling observation. Under confinement, solitons drift slowly to a particular position in the trough, namely, the center when the basin is correctly leveled [24]. This result contradicts the virtual-pair model, which identifies the center as an unstable position.

To explore this further, we ran experiments in a Plexiglas trough of dimensions $l = 49.9$ cm and $b = 25.4$ mm filled with water and 2 ml of Photo-Flo to a depth of $d = 20$ mm. The basin was attached to an electromechanical shaker. Its vertical acceleration is given by $a(t) = a_0 \sin 2\pi f t$, where f is the forcing frequency. Some ink drops were added for visualization. The first transverse-mode frequency in the trough was found to be $f_{0,1} = 5.49$ Hz. The system mechanical response was recorded using a piezoelectric accelerometer fixed to the basin. A high-speed camera was arranged to acquire front views [see Fig. 1(b)] and was synchronized with the external driving so the double-period oscillation of solitons appeared to be locked during acquisitions. Solitons appeared at frequencies f slightly lower than $2f_{0,1} \approx 11.00$ Hz and vertical acceleration amplitudes a_0 around $0.1g$. To depict the structures' spatiotemporal behavior, we obtained the interface position along the basin using an image processing technique described elsewhere [24].

Since we are interested in isolating soliton-wall interactions, we designed a very simple protocol: a soliton was created ($f = 5.25$ Hz and $a_0 = 0.105g$) in a subdomain of the trough and allowed to relax slowly to its equilibrium position. Afterwards, we inserted a vertical Plexiglas slab of thickness 3 mm and breadth $\approx b$ at a certain position x^*. The slab touched the basin bottom so the fluid layer was divided into two subdomains, as displayed in Fig. 1. The slab was then kept in its position until the end of acquisitions. Under this configuration, the inserted slab mimics a new boundary wall that suddenly reduces the soliton domain.

After inserting the slab, the soliton was instantly pushed back from the slab and started to drift to a new equilibrium position in the basin. We depict an example of this behavior in Fig. 2(a) where the evolution recalls the spatiotemporal snapshots reported for tilted troughs [24]. Notice that a second soliton was kept in a separate subdomain for records. Its trajectory was barely affected by the main soliton interaction. It should be remarked that all these experiments were performed in a region of parameters where steady bound-pair states do not occur at all, differing from the experiments in Ref. [16]. Actually, the boundary-wall interaction in Fig. 2(a) is consistent with the protocol in Ref. [22] for trapping solitons, which exploited a region of parameters where wall-repulsion and pair-attraction behavior coexist. In Fig. 2(b) we depict another experiment ($f = 5.25$ Hz and $a_0 = 0.108g$): a steady state of two opposite-sign solitons was disrupted by the insertion of a wall. In a similar way to Fig. 2(a), the two solitons are

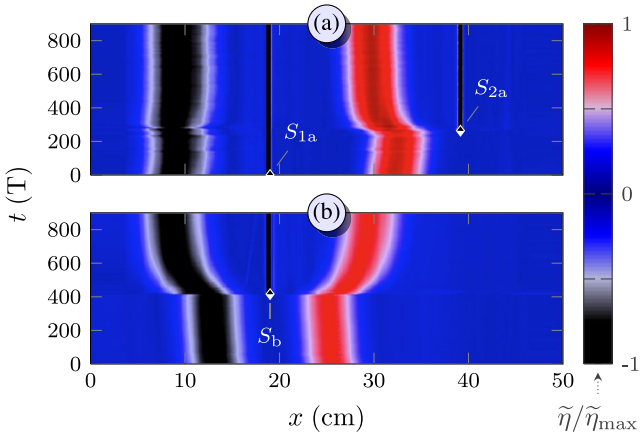

FIG. 2 (color online). Two spatiotemporal diagrams uncovering experimental soliton-wall interactions. The time t is expressed in terms of the period T and $\tilde{\eta}$ is normalized. (a) A slab S_{1a} divides the cell into two parts, each containing a soliton. Then, a second slab S_{2a} is inserted, repelling the right soliton and barely disturbing the other one. (b) A slab S_b is inserted between two solitons with opposite signs, inducing a sudden repulsion.

immediately pushed back instead of being attracted, showing clearly that walls and virtual pairs are not equivalent.

The answer for explaining this effect comes from an overlooked extra dissipation taking place at the boundary layer on the lateral walls. To give a simple explanation, let us first remark on the resemblance between our system and a chain of forced nonlinear oscillators (see Fig. 3). According to Eq. (1), each oscillator can be characterized by three parameters: ν, γ, and μ. Neighbor coupling is achieved via the dispersion term. The first parameter ν depends on the forcing and the transverse-mode natural frequency. Since any of these variables depend on the oscillator position along the chain, the detuning of all the oscillators is the same. A similar argument stands for the forcing amplitude but not for the damping term: the contact with lateral walls induces an extra dissipation in the oscillators placed at the edges.

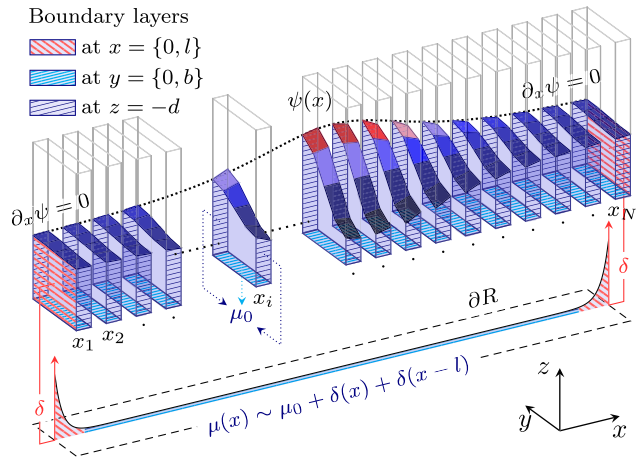

FIG. 3 (color online). A nonpropagating hydrodynamic soliton as a chain of N coupled oscillators. Dissipation occurs at boundary layers surrounding the fluid. All the oscillators along the chain contain boundary layers at $y = \{0, b\}$ and $z = -d$, but only those at $x_{\{1,N\}}$ contain lateral boundary layers. This induces higher damping rates when approaching edges (see μ curve below).

The way that standing waves dissipate energy in closed basins was analyzed in Ref. [31]. Velocity fields beneath standing waves display potential features inside the bulk with thin shearing layers along the boundaries. Considering that energy dissipation mainly occurs there, the damping term in Eq. (1) is the sum of contributions from (i) boundary layers at the rigid boundaries, (ii) boundary layers at the free surface, and (iii) capillary hysteresis of the menisci, i.e., $\mu = \mu_W + \mu_S + \mu_L$. For the sake of simplicity, herein we only analyze the μ_W term—similar procedures can used for μ_S and μ_L corrections.

Consider a uniform fluid layer of kinematic viscosity ν^* surrounded by vertical walls and whose horizontal section is R. The layer supports standing waves characterized by the velocity potential ϕ at $z = 0$ and the frequency ω, which are related uniquely to the patterns $\eta_{p,q}$. The quantity μ_W is proportional to a small dimensionless parameter $\epsilon_\nu \equiv (2\nu^*/\omega)^{1/2}k$, while the constant of proportionality is

$$\mu'_W = \frac{J+K}{8} + \frac{1-\tau^2}{4\tau}\left[1 - kd\left(\frac{J-K}{2}\right)\right], \qquad (3)$$

where $\tau = \tanh(kd)$. Further details can be found in the Supplemental Material [32] and Refs. [31,33]. The expression depends on three form factors: $J \equiv kI^{-1}\int_{\partial R} d\ell|\phi|^2$, $K \equiv (kI)^{-1}\int_{\partial R} d\ell|\partial_\ell\phi|^2$, and $I \equiv \iint_R dxdy|\nabla\phi|^2$. The terms proportional to J and K arise from boundary layers at vertical walls while the remaining ones come from the bottom boundary layer (I is proportional to the energy supported by the wave).

The current approach for determining μ_W for nonpropagating hydrodynamic solitons [14] assumes a basin of infinite extent in the x direction. Thus $d\ell = dx$ in J and K form factors and $I = \int(\int_0^b |\nabla\phi|^2 dy)dx$ (see Fig. 1). Recalling that ϕ is the crossed waveform, and hence $\phi(x, y) \sim \cos ky$, it follows that $J = 4\pi^{-1}$ and $K = 0$. The value obtained for μ_W under these assumptions is the same despite the limits of integration in the x direction. This is in apparent agreement with our chain of identical coupled oscillators from Eq. (1).

However, when approaching a lateral wall in a finite basin, the integrals J and K display a jump due to the extra lateral path along ∂R in the y direction (see Fig. 3). Clearly the calculations taking into account the $\eta_{0,1}$ mode within a finite container yield a global decay rate μ_W that does not seem appropriate for localized structures. For solitons, as in a chain of nonlinear oscillators, we require a local damping coefficient. A better approach is to consider

$\phi(x,y) = \psi(x)\cos(ky)$ and write the extra integral terms in J and K due to lateral walls as $\int_{\partial R} d\ell = \int_0^l \int_0^b [\delta(x) + \delta(x-l)]dydx$. As both the numerator and denominator in J are proportional to $|\psi|^2$ and include integrals along x, local dissipation can be found by dropping integrals along x. Physically, this is equivalent to deriving a local coefficient from the ratio of local dissipation and local energy along the x direction through a limit process where the oscillators' thicknesses become infinitely small. Integrating in y, we finally find

$$\mu'_W = \frac{1}{2\pi} + \frac{\pi - 2kd}{2\pi\sigma} + \frac{\sigma - 2kd}{4k\sigma}[\delta(x) + \delta(x-l)], \quad (4)$$

where $\sigma \equiv \sinh 2kd$. The details are also available in the Supplemental Material [32]. The third term is the correction for the damping coefficient. It is zero along the chain and diverges when approaching lateral walls. Notice that the existence of such a singularity does not pose any problem from the physics point of view. Its extent—although negligible compared to the soliton length scale—is finite and equal to the boundary-layer thickness. To sum up, we showed from fluid dynamics that, within the amplitude equation, physical boundary conditions cannot be modeled by classical ones. This is achieved instead via the spatially nonuniform $\mu(x)$ from Eq. (4).

The question now is, what happens to solitons from Eq. (2) when adding Dirac delta terms via μ in Eq. (1)? The scenario brings to mind forced coupled-pendula chains doped with impurities, i.e., larger (shorter) pendula [25,34,35], which are known to repel (attract) solitons for negative detuning ν. Notice that in that case, singular discrete functions arise in the ν coefficient as the local natural frequency changes with pendulum length. In our case, the mechanism is completely different as it emerges inherently from confinement.

To answer the question, we made numerical simulations of the pd-NLS model [Eq. (1)], replacing μ as a function of space $[\mu \to \mu(x)]$ on a 120-point spatial domain ($dx = 0.3$ cm) using classical Runge-Kutta routines for time integration ($dt = 10^{-2}T$). We used the formulas in Ref. [14] to obtain μ, ν, and γ from the experimental physical quantities. Just as in our physical setup, our code allows us to insert slabs within the spatial domain. These—like the walls—are modeled by locally imposing the impermeability boundary condition. Likewise, Gaussians ($\sigma = 0.5$ cm and amplitude δ_μ) centered at correspondent locations mimic the Dirac-delta corrections in the damping coefficient from Eq. (4). Figure 4 displays several numerical experiments that evidence huge differences in long-time-scale behavior between our model (in main figures) and the classical one (in insets). While the classical model yields different types of bound states, ours generates an equilibrium state driven by soliton-wall repulsion where finally each soliton is centered in its subdomain [see, e.g., Fig. 2(a)]. Boundary layers have an effect on system

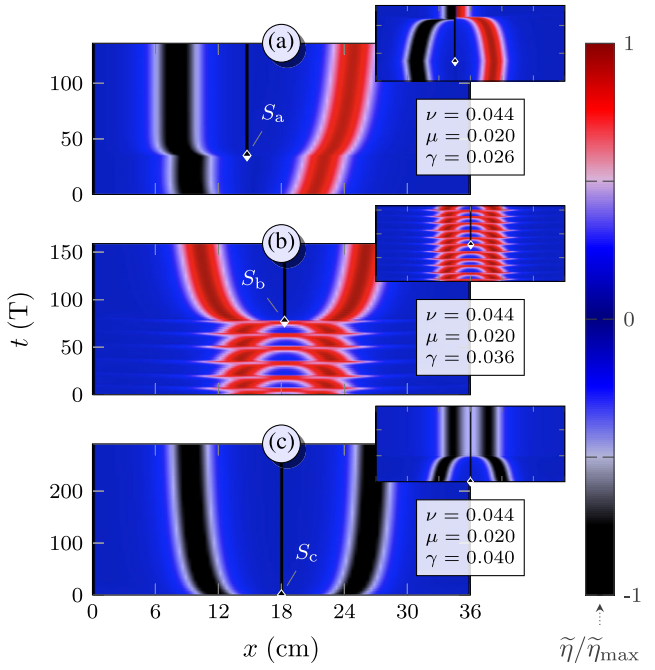

FIG. 4 (color online). Spatiotemporal diagrams of numerical runs that evidence the dominance of dissipation in soliton-wall interactions at long time scales for three sets of (ν, μ, γ) and $\delta_\mu = 0.3$. The insets displays simulations under the classical approach ($\delta_\mu = 0$). (a) The sudden insertion of a slab S_a repels a pair of opposite-sign solitons rather than attracting them. (b) A slab S_b breaks an oscillating same-sign pair instead of holding the state. Likewise, in (c) the slab avoids the formation of a same-sign steady bound state.

dynamics regardless of their infinitesimal extent and despite the system length. The key for understanding this is overlapping functions. While in classical systems long-range interactions arise from a long-range field overlapping a punctual particle, in ours the long-range tail of an extended particle, $\psi(x)$, overlaps a field with punctual features, $\mu(x)$. The similitude between Figs. 2(b) and 4(a), as well as the differences with the latter's inset, show plainly that the dissipative process described in this Letter rules the confined solitons' spatiotemporal behavior. The model not only solves the slow drifts from Ref. [24] but also yields soliton-wall bound states in the region of parameters where they were reported (cf. Ref. [27]).

The identified mechanism can be useful to understand the effects of boundaries on other parametric dissipative systems. Regardless of the particular physical origin, the idea of damping-coefficient jumps at boundaries is fundamental. It does not stand only for hydrodynamic solitons [9–11], but also, for instance, for granular ones [7], where the jump will be due to extra friction between grains and walls. Notice that in any case, the mechanism does not depend on how energy is pumped. Instead, the cornerstone of the raised-out jumps is the inherent dissipative nature of systems. Hence, similar phenomena can also be expected in nonparametric dissipative solitons such as *convectons* [1],

where numerical simulations of the full-equation problem with physical boundary conditions [36] provide results in line with ours (e.g., centered steady states).

To conclude, we have analyzed experimentally and theoretically the interaction between nonpropagating hydrodynamic solitons and walls. Our research was motivated by unattended issues about soliton confinement in laboratory experiments. We showed that soliton-wall interactions are driven by a dissipative mechanism that can substantially alter the system dynamics at long time scales. Within the pd-NLS classical model, we demonstrated that thin boundary layers on walls induce a jump in the local damping coefficient. Using numerical simulations, we showed that this generates soliton repulsion, triggering a slow drift to the midpoint of each soliton domain. Besides the good agreement with experimental observations, our results provide two fundamental lessons to be considered further. First, damping in amplitude equations may be tricky; its spatial independence can be broken down by the inherent system configuration, e.g., confinement. This is an issue common to experiments in dissipative out-of-equilibrium systems. Second, as for other parameters in amplitude equations [25,26], damping spatial dependence has an impact on localized solutions. Even highly localized subtle effects can absolutely modify the system's final outcome.

We thank R. Silva and C. Pinochet for their technical help. M. A. G-N. acknowledges the financial support of FONDECYT project 3110024. L. G. was supported by CONICYT grants 24100131/57080094 and the AXA Research Fund. The research was also financed by the project ACT-127. The authors are grateful to Prof. N. Mujica and M. Clerc for fruitful discussions.

*Present address: Laboratoire "Matière et Systèmes Complexes" (MSC), UMR 7057 CNRS, Université Paris 7 Diderot, 75205 Paris Cedex 13, France.
leonardo.gordillo@univ-paris-diderot.fr
†monica.garcia@ucv.cl

[1] J. J. Niemela, G. Ahlers, and D. S. Cannell, Phys. Rev. Lett. **64**, 1365 (1990).
[2] N. Akhmediev and A. Ankiewicz, *Dissipative Solitons* (Springer, Heidelberg, 2005).
[3] B. Denardo, B. Galvin, A. Greenfield, A. Larraza, S. J. Putterman, and W. B. Wright, Phys. Rev. Lett. **68**, 1730 (1992).
[4] I. V. Barashenkov, M. M. Bogdan, and V. I. Korobov, Europhys. Lett. **15**, 113 (1991).
[5] J. N. Kutz, W. L. Kath, R.-D. Li, and P. Kumar, Opt. Lett. **18**, 802 (1993).
[6] S. Longhi, Opt. Lett. **20**, 695 (1995).
[7] P. B. Umbanhowar, F. Melo, and H. L. Swinney, Nature (London) **382**, 793 (1996).
[8] O. Lioubashevski, Y. Hamiel, A. Agnon, Z. Reches, and J. Fineberg, Phys. Rev. Lett. **83**, 3190 (1999).
[9] H. Arbell and J. Fineberg, Phys. Rev. Lett. **85**, 756 (2000).
[10] M. Shats, H. Xia, and H. Punzmann, Phys. Rev. Lett. **108**, 034502 (2012).
[11] J. Rajchenbach, A. Leroux, and D. Clamond, Phys. Rev. Lett. **107**, 024502 (2011).
[12] J. Wu, R. Keolian, and I. Rudnick, Phys. Rev. Lett. **52**, 1421 (1984).
[13] M. Umeki, J. Phys. Soc. Jpn. **60**, 146 (1991).
[14] J. W. Miles, J. Fluids Mech. **148**, 451 (1984).
[15] X. Wang and R. Wei, Phys. Lett. A **192**, 1 (1994).
[16] W. Wang, X. Wang, J. Wang, and R. Wei, Phys. Lett. A **219**, 74 (1996).
[17] I. V. Barashenkov, S. R. Woodford, and E. V. Zemlyanaya, Phys. Rev. Lett. **90**, 054103 (2003).
[18] M. G. Clerc, S. Coulibaly, N. Mujica, R. Navarro, and T. Sauma, Phil. Trans. R. Soc. A **367**, 3213 (2009).
[19] S. Longhi, Phys. Rev. E **53**, 5520 (1996).
[20] I. V. Barashenkov, Y. S. Smirnov, and N. V. Alexeeva, Phys. Rev. E **57**, 2350 (1998).
[21] X. Wang, Physica (Amsterdam) **154D**, 337 (2001).
[22] M. G. Clerc, S. Coulibaly, L. Gordillo, N. Mujica, and R. Navarro, Phys. Rev. E **84**, 036205 (2011).
[23] J. Yan, C. Zhou, and J. You, Phys. Fluids A **4**, 690 (1992).
[24] L. Gordillo, T. Sauma, Y. Zárate, I. Espinoza, M. G. Clerc, and N. Mujica, Eur. Phys. J. D **62**, 39 (2011).
[25] N. V. Alexeeva, I. V. Barashenkov, and G. P. Tsironis, Phys. Rev. Lett. **84**, 3053 (2000).
[26] W. Chen, L. Lu, and Y. Zhu, Phys. Rev. E **71**, 036622 (2005).
[27] X. Wang, J. Acoust. Soc. Am. **104**, 715 (1998).
[28] H. Lamb, *Hydrodynamics*, 6th edition (Cambridge University Press, Cambridge, England, 2006).
[29] M. Faraday, Phil. Trans. R. Soc. London A **121**, 299 (1831).
[30] I. V. Barashenkov and E. V. Zemlyanaya, Phys. Rev. E **83**, 056610 (2011).
[31] J. W. Miles, Proc. R. Soc. A **297**, 459 (1967).
[32] See Supplemental Material at http://link.aps.org/supplemental/10.1103/PhysRevLett.112.164101 for a detailed calculation of μ_W and the form factors I, J, and K.
[33] L. Gordillo, Ph. D. thesis, Universidad de Chile, Santiago, 2012.
[34] O. M. Braun and Y. S. Kivshar, Phys. Rev. B **43**, 1060 (1991).
[35] W. Chen, Y. Zhu, and L. Lu, Phys. Rev. B **67**, 184301 (2003).
[36] I. Mercader, O. Batiste, A. Alonso, and E. Knobloch, J. Fluids Mech. **667**, 586 (2011).